



RESEARCH LETTER

10.1002/2017GL074273

Key Points:

- Realistic simulation of the hiatus in global mean surface temperature is no guarantee that the pattern of temperature trends is reproduced
- Dynamically induced cooling over Eurasia and North America is driven by internal atmospheric dynamics and tropical Pacific teleconnections
- Hiatus in global mean surface temperature is due equally to cooling from internal atmospheric dynamics and tropical Pacific teleconnections

Supporting Information:

- Supporting Information S1

Correspondence to:

C. Deser,
cdeser@ucar.edu

Citation:

Deser, C., R. Guo, and F. Lehner (2017), The relative contributions of tropical Pacific sea surface temperatures and atmospheric internal variability to the recent global warming hiatus, *Geophys. Res. Lett.*, *44*, doi:10.1002/2017GL074273.

Received 23 MAY 2017

Accepted 20 JUL 2017

Accepted article online 25 JUL 2017

The relative contributions of tropical Pacific sea surface temperatures and atmospheric internal variability to the recent global warming hiatus

Clara Deser¹ , Ruixia Guo^{1,2} , and Flavio Lehner¹ 

¹Climate and Global Dynamics Division, National Center for Atmospheric Research, Boulder, Colorado, USA, ²Key Laboratory for Semi-Arid Climate Change of the Ministry of Education and College of Atmospheric Sciences, Lanzhou University, Lanzhou, China

Abstract The recent slowdown in global mean surface temperature (GMST) warming during boreal winter is examined from a regional perspective using 10-member initial-condition ensembles with two global coupled climate models in which observed tropical Pacific sea surface temperature anomalies (TPAC SSTAs) and radiative forcings are specified. Both models show considerable diversity in their surface air temperature (SAT) trend patterns across the members, attesting to the importance of internal variability beyond the tropical Pacific that is superimposed upon the response to TPAC SSTA and radiative forcing. Only one model shows a close relationship between the realism of its simulated GMST trends and SAT trend patterns. In this model, Eurasian cooling plays a dominant role in determining the GMST trend amplitude, just as in nature. In the most realistic member, intrinsic atmospheric dynamics and teleconnections forced by TPAC SSTA cause cooling over Eurasia (and North America), and contribute equally to its GMST trend.

1. Introduction

The well-documented pause or slowdown in global-mean surface warming during the early part of this century, hereafter termed the “hiatus,” has been primarily attributed to internal climate variability with a small (10–15%) contribution from natural (volcanic aerosols and insolation) radiative forcing [i.e., *Kosaka and Xie*, 2013 (hereafter KX13); *Huber and Knutti*, 2014; *Marotzke and Foster*, 2015; *Fyfe et al.*, 2016; *Hu and Fedorov*, 2017]. In combination, these influences counteracted the warming effect of rising greenhouse gas (GHG) concentrations, effectively stalling the rate of increase of global-mean surface temperature (GMST). While GMST is a fundamental metric for defining the hiatus, obeying global energetic constraints and facilitating conceptual understanding, it masks important spatial and seasonal variation for which a more detailed mechanistic explanation is needed. As many studies have shown, the hiatus is primarily a boreal winter phenomenon of the Northern Hemisphere (NH) continents, with cooling over Eurasia making the dominant contribution [i.e., *Cohen et al.*, 2012; KX13; *Trenberth et al.*, 2014; *Saffioti et al.*, 2015; *Li et al.*, 2015; *Huang et al.*, 2017]. The proximate cause of the Eurasian winter cooling is a trend in the large-scale atmospheric circulation toward enhanced anticyclonic conditions accompanied by more frequent submonthly blocking episodes [previous references and *Luo et al.*, 2016]. Understanding the origin of this circulation trend is thus critical to explaining the hiatus.

Many studies have focused on the role of the tropical Pacific in the hiatus, in particular a cooling of the upper ocean mixed layer and accompanying changes in winds and rainfall [i.e., KX13; *Trenberth et al.*, 2014; *England et al.*, 2014; *Watanabe et al.*, 2014; *Dai et al.*, 2015]. These tropical Pacific climate anomalies are part of a pan-Pacific structure of internal variability termed the “Pacific Decadal Oscillation/Interdecadal Pacific Oscillation” (PDO/IPO) [*Mantua et al.*, 1997; *Power et al.*, 1999]. Quantitative evidence for the dominant role of the tropical Pacific was first demonstrated by KX13 based on a novel set of coupled model experiments, and confirmed by *England et al.* [2014] and *Watanabe et al.* [2014] using slightly different experimental approaches. More generally, the PDO/IPO has been linked to earlier periods of accelerated and decelerated global-mean surface warming since the midnineteenth century [*Kosaka and Xie*, 2016, and references therein; hereafter KX16]. Although the tropical Pacific has been implicated in nearly all studies of the hiatus, other sources of internal variability including atmospheric dynamics [*Li et al.*, 2015] and the Atlantic Multidecadal Oscillation [*Chen and Tung*, 2014] have also been shown to contribute. Finally, *Douville et al.* [2015] caution that model error may compromise the ability of models to discriminate among the different factors.

In this study, we revisit the role of eastern tropical Pacific sea surface temperature anomalies (SSTAs) to the hiatus from a regional perspective, using the experimental protocol of KX13 applied to two global coupled climate models. However, unlike KX13 whose primary focus was on GMST, we emphasize the spatial pattern of SAT trends that make up the global mean. As we shall show, realistic simulation of the GMST trend is no guarantee that the geographical structure of SAT trends is reproduced, calling into question whether the model “gets the right answer for the right reason”. In particular, we discriminate between the influences of observed internally generated tropical Pacific SSTA and simulated internal atmospheric variability on both GMST and the spatial pattern of SAT trends. As such, our study fills the gap between *Li et al.* [2015], who investigated the relative roles of internal atmospheric variability and Arctic sea ice loss on the spatial pattern of SAT trends and KX13 who emphasized the relative contributions of tropical Pacific SSTA and radiative forcing on GMST. We focus on boreal winter, the season with the most pronounced hiatus [i.e., *Cohen et al.*, 2012] (Figure S1 in the supporting information).

The rest of the paper is organized as follows: the models, experimental design, analysis methods, and observational data sets are described in section 2. Results are presented in section 3, and summarized and discussed in section 4.

2. Models and Experimental Design, Analysis Methods, and Observational Data

2.1. Models and Experimental Design

We analyze output from two 10-member coupled model ensembles of tropical Pacific “Pacemaker” simulations, one performed with the Geophysical Fluid Dynamics Laboratory Coupled Model version 2.1 (GFDL CM2.1; the same model used in KX13 and KX16) and the other with the National Center for Atmospheric Research Community Earth System Model version 1 (NCAR CESM1) [*Kay et al.*, 2015]. In these simulations, the temporal history of SSTA in the eastern tropical Pacific (15°S–15°N, 180°W to the coast of South America, with a linearly tapering buffer zone of 5° in all directions) is nudged to observations (NOAA Extended Reconstruction Sea Surface Temperature, version 3 (ERSSTv3b)) [*Smith et al.*, 2008], leaving the rest of the model’s coupled climate system free to evolve. Note that only the SSTA, not the total SST, is nudged to observations, maintaining the model’s mean state including any model biases. All simulations are subject to the historical evolution of radiative forcing through 2005, and the Representative Concentration Pathway version 8.5 (RCP8.5) (RCP4.5) radiative forcing specification thereafter for CESM1 (CM2.1) following the fifth phase of the Coupled Model Intercomparison Project protocols [*Taylor et al.*, 2012]. Ensemble spread is created by introducing a random atmospheric temperature perturbation at the level of round-off error (10^{-14} °C) on the first day of the simulation (1 January 1880 in the case of CM2.1 and 1 January 1920 in the case of CESM1). The atmospheric and land model components of CESM1 (CM2.1) have a horizontal resolution of 1° in latitude and 1° in longitude (2° in latitude and 2.5° in longitude). Further details on the models and simulations are provided in *Deser et al.* [2017]. We note that while the SSTA nudging procedure does not conserve heat, it has the advantage over the “wind nudging” protocol [*England et al.*, 2014; *Watanabe et al.*, 2014] by ensuring a realistic evolution of SSTA in the eastern tropical Pacific. Further, as noted by KX16, the artificial heat introduced to the ocean-atmosphere system by the SSTA nudging procedure is smaller than the top-of-atmosphere radiation imbalance (TOARI), and their sum is within the ensemble spread of the TOARI of the free-running simulations.

In addition to the Pacemaker simulations, we make use of historical and RCP (4.5 for CM2.1 and 8.5 for CESM1) simulations with the free-running (i.e., unnudged) versions of these models, of which there are 20 members for CM2.1 and 40 members for CESM1. For clarity, we note that all CM2.1 simulations analyzed here are those presented in KX16. However, KX16’s analysis of these simulations took a general view of the role of the tropical Pacific as a modulator of the rates of annual-mean global surface warming during 1880–2013, using 15 year trends as a metric, rather than focusing specifically on the recent hiatus in boreal winter. We also note that KX13’s CM2.1 simulations used a slightly different region for the SSTA restoring as well as a different observational SST data set for the restoring.

We also make use of a 2600 year preindustrial (constant 1850 radiative conditions) control simulation conducted with the atmosphere-land model components of CESM1 (hereafter referred to as Community Atmospheric Model version 5 or CAM5) using a prescribed repeating seasonal cycle of SSTs and sea ice conditions taken from the long-term climatology of a companion 2200 year preindustrial control run of the fully coupled CESM1 [see *Kay et al.*, 2015]. This lengthy atmosphere-only control simulation provides

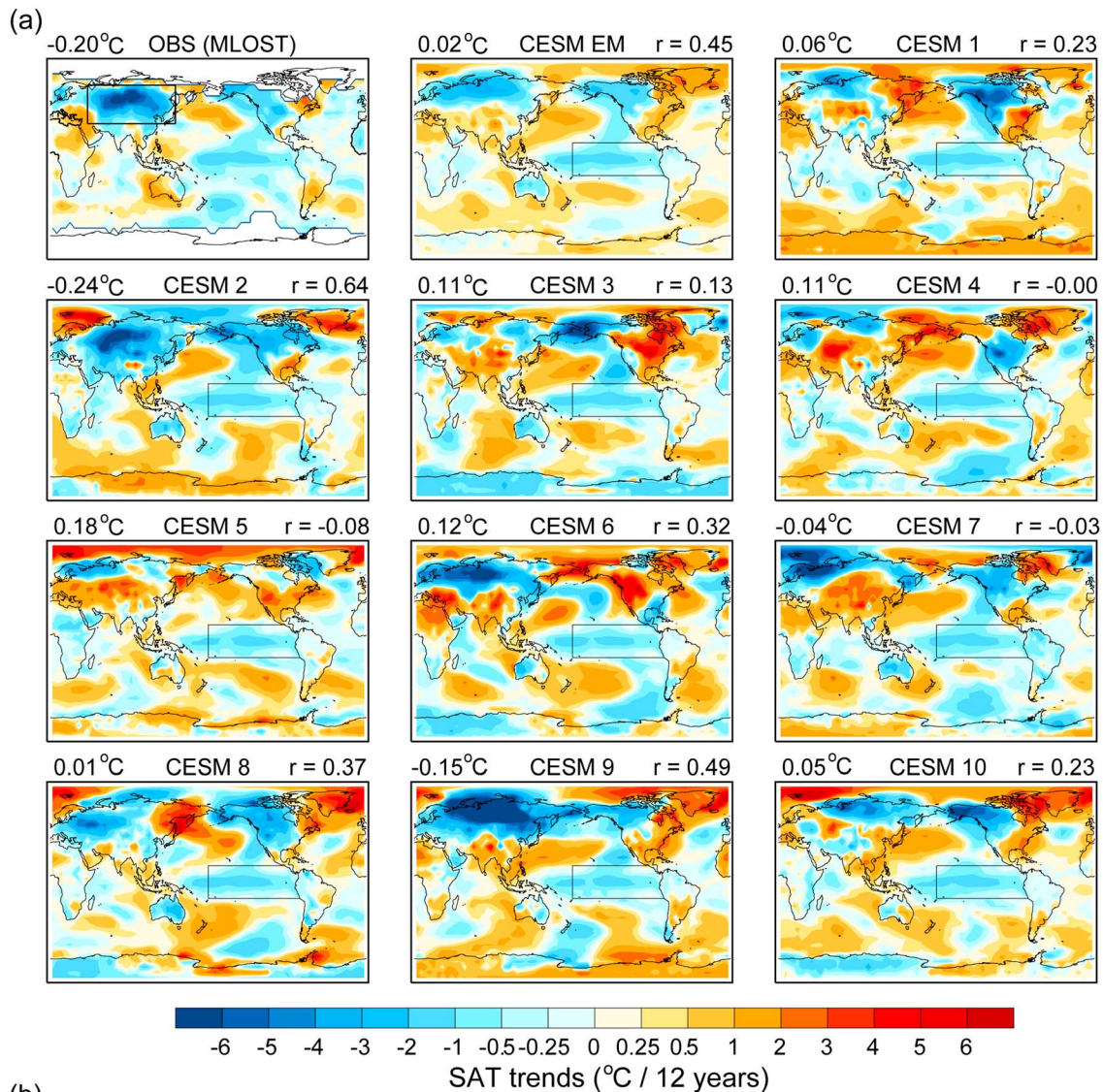


Figure 1. (a) DJF SAT trends (2002–2013; $^{\circ}\text{C}/12$ years) from observations (MLOST), the ensemble mean of the 10 CESM1 Pacemaker simulations (CESM EM) and each individual simulation (CESM 1–10). The numbers in the top left and right corners denote the GMST trend value, masked by the spatial coverage in MLOST, and the pattern correlation (r) with MLOST, respectively. The gray boxes show the area used for the SSTA nudging, and the black box in the top left shows the area referred to as “Eurasia” in the text. (b) Same as in Figure 1a but for zonal-mean SAT trends weighted by cosine of latitude. MLOST is shown in black, CESM EM in red, and the individual simulations in gray (ensemble member 2 is highlighted in blue).

robust statistics on the variability created solely by the atmosphere and land. We have no analogous simulation with CM2.1.

2.2. Analysis Methods

We focus on the 3 month season December-January-February (DJF) and compute linear trends over the hiatus period of 2002–2013, where 2002 is defined as December 2001, January 2002, and February 2002 and 2013 is defined as December 2012, January 2013, and February 2013. This time period was chosen to match KX13, and avoids undue influence from the record El Niño event of 1997–1998 and subsequent 3 year La Niña event of 1999–2001 [KX13; see also *Fyfe et al.*, 2016]. The hiatus ended in 2013 due to the onset of El Niño in 2014 [*Hu and Federov*, 2017]; therefore, we choose 2013 as the final year of our hiatus period. However, virtually identical results are obtained using 2012 as the final year, as in KX13 (not shown). Of the four seasons, DJF shows the greatest slowdown in global surface warming even when compared with the rate of warming during previous decades [*Li et al.*, 2015] (Figure S1).

2.3. Observational Data Sets

Our primary SAT data set is the Merged Land-Ocean Surface Temperature (MLOST) analysis version 3.5 [*Vose et al.*, 2012] on a 5° latitude × 5° longitude grid. This data set combines land SATs from the Global Historical Climatology Network Monthly version 3 with SSTs from ERSSTv3b. We use MLOST for compatibility with the Pacemaker simulations, which were nudged to ERSSTv3b in the eastern tropical Pacific. However, similar results are obtained with five other SAT data sets (Figure S2), consistent with *Fyfe et al.* [2016]. Sea level pressure (SLP) was obtained from the ERA-Interim Reanalysis Product [*Dee et al.*, 2011] on a 1° latitude × 1° longitude grid.

3. Results

Global DJF SAT trend (2002–2013) maps based on observations (MLOST) and each of the 10 CESM1 Pacemaker simulations are compared in Figure 1. The GMST trend value and pattern correlation (r) against MLOST are given in the top left and right corners, respectively (note that the model is masked by the MLOST coverage for both calculations). The Pacemaker ensemble members show considerable diversity in their trend patterns and amplitudes, particularly in the extratropics. For example, some depict strong cooling over Eurasia (in excess of -6°C in runs 2, 6, 7, and 9), while others show almost no change or even warming in this region (runs 3 and 4, respectively; note that all trend values are understood to be in units of per 12 years). Similarly, trends over North America range from strongly positive (runs 3 and 6) to negative in many others. Trends over the ocean show less diversity, especially over the North Pacific, although this is not always the case (run 5 for example). Recall that the diversity of responses across the Pacemaker ensemble is entirely a result of internal variability beyond that forced from the tropical Pacific. This diversity results in a range of GMST trends, from -0.24°C in run 2 to a $+0.18^{\circ}\text{C}$ in run 5, and a range of pattern correlations, from -0.08 in run 5 to $+0.64$ in run 2. In terms of these dual metrics, run 2 shows the greatest correspondence to MLOST and run 5 the least.

Latitudinal profiles of the simulated and observed (MLOST) SAT trends, weighted by cosine of latitude to preserve relative area, are compared in Figure 1b. The largest spread across the CESM1 Pacemaker ensemble occurs over the NH extratropics, consistent with the visual impression from Figure 1a. As before, run 2 shows the closest resemblance to MLOST (and the other SAT data sets; Figure S2); in particular, the largest zonal-mean contribution to the GMST cooling trend occurs in the latitude band 40° – 65°N , with maximum values of approximately -1.25°C compared to -0.90°C for MLOST. The cooling in this latitude band comes almost entirely from land (Figure S3). Similar results were shown in *Li et al.* [2015], but for discrete 30° latitudinal bands.

The ensemble mean of the 10 CESM1 Pacemaker simulations (denoted CESM1_EM), which can be interpreted as an estimate of the model's forced response to radiative changes plus observed tropical Pacific SST variability, shows a similar pattern of SAT trends as MLOST over much of the extratropical NH (albeit northward shifted compared to MLOST; see Figure 1b), including the band of negative values over Eurasia and western North America, with less correspondence over the extratropical Southern Hemisphere, for an overall pattern correlation of 0.45 (Figure 1a). The GMST trend in CESM1_EM is $+0.02^{\circ}\text{C}$ compared to -0.20°C in MLOST.

Analogous trend maps for the CM2.1 Pacemaker ensemble are shown in Figure 2a. Like CESM1, there is large spread among the individual CM2.1 ensemble members. However, no single CM2.1 simulation resembles

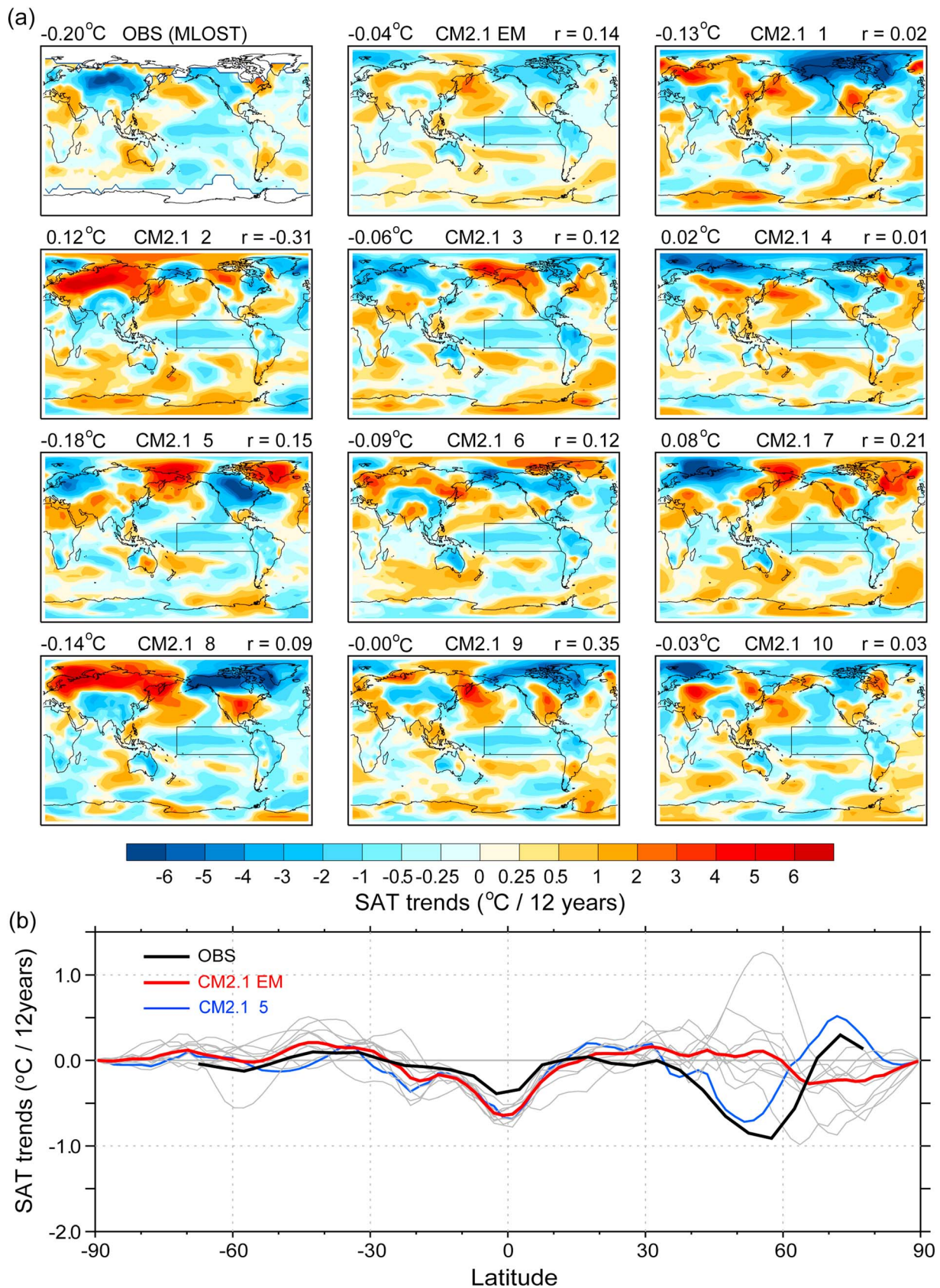


Figure 2. (a and b) Same as in Figure 1 but for the GFDL CM2.1 Pacemaker simulations. In Figure 2b, ensemble member 5 is highlighted in blue.

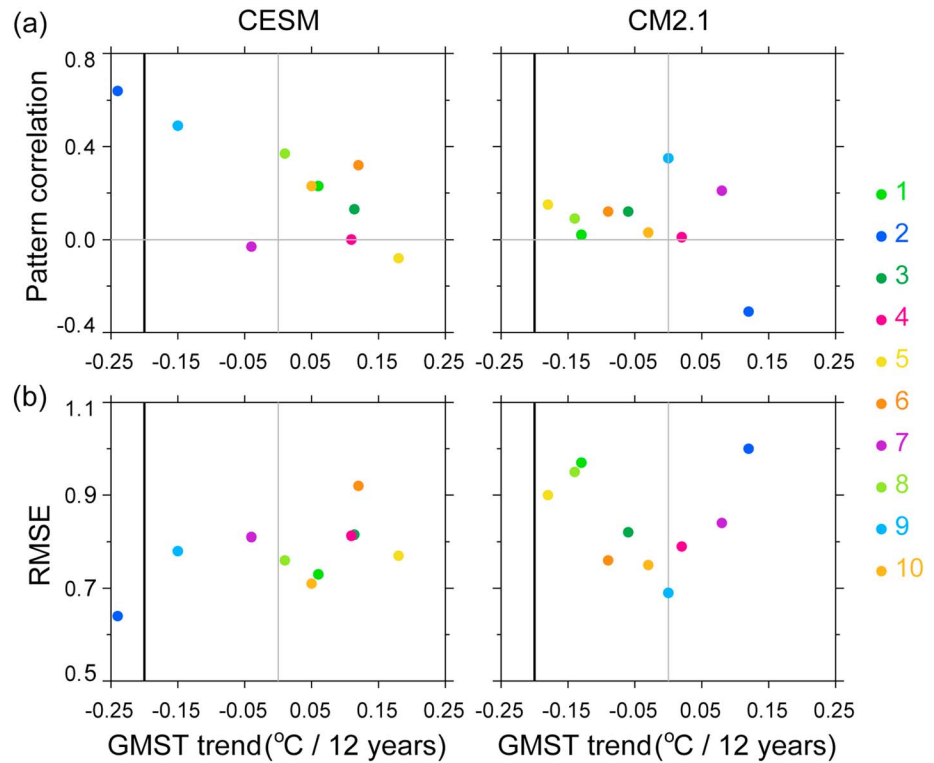


Figure 3. (a) Scatterplots of the pattern correlation between DJF SAT trends in observations (MLOST) and each of the (left) CESM1 and (right) CM2.1 Pacemaker simulations (y axis) against the simulated DJF GMST trend (°C/12 years; x axis). The vertical black line denotes the MLOST GMST trend. Color coding for the 10 simulations is given in the legend to the right. (b) Same as in Figure 3a but for RMSE (°C/12 years) in place of pattern correlation, where RMSE is computed from area-weighted differences between the simulated and MLOST SAT trends.

observations as closely as the most realistic CESM1 simulation: the highest pattern correlation with MLOST is 0.35 (CM2.1 run 9) compared to 0.64 for CESM1 (run 2). Note that although CM2.1 run 5 shows a “realistic” latitudinal profile of SAT trends over the NH extratropics, this is misleading because the cooling occurs mainly over North America rather than Eurasia (Figure 2b); further, this run shows a low pattern correlation ($r = 0.15$) with MLOST. Unlike CESM1_EM, the ensemble mean of the 10 CM2.1 Pacemaker simulations (CM2.1_EM) lacks a cooling trend over Eurasia, and exhibits a weaker pattern correlation with MLOST ($r = 0.14$). The GMST trend in CM2.1_EM is -0.04°C .

Is there a relationship between the realism of the SAT trend patterns and GMST trend values in the Pacemaker ensembles? CESM1 shows a quasi-linear relationship between pattern correlation (against MLOST) and GMST trend, while CM2.1 shows a pattern correlation that is largely independent of GMST trend (Figure 3a). Furthermore, the CESM1 members with the highest pattern correlation also show the lowest RMSE of their SAT trends with respect to MLOST, and the most realistic GMST trend values (Figure 3b). In contrast, the CM2.1 ensemble members with the most realistic GMST trends have some of the highest RMSE values (Figure 3b) and lowest pattern correlations (Figure 3a). Thus, GMST trends may mask discrepancies in the geographical pattern and local amplitude of SAT trends relative to observations in the CM2.1 ensemble more so than in the CESM1 ensemble.

As discussed earlier, cooling over the NH continents and especially Eurasia played a dominant role in the hiatus. This is evident in the SAT trend maps based on MLOST (Figure 1) and all other data sets examined (Figure S2). More quantitatively, Eurasia ($30^{\circ}\text{--}70^{\circ}\text{N}$, $40^{\circ}\text{--}140^{\circ}\text{E}$) accounts for 71% of the hiatus in DJF GMST (MLOST) despite covering such a small fractional area of the globe (6%). In the most realistic of the Pacemaker simulations (member 2 of CESM1; recall Figure 3), Eurasia accounts for a similar proportion (72%) of the simulated GMST trend. More generally, SAT trends over Eurasia are well correlated with GMST trends across the CESM1 ensemble ($r = 0.75$) and only weakly correlated across CM2.1 ($r = 0.26$; Figure S4).

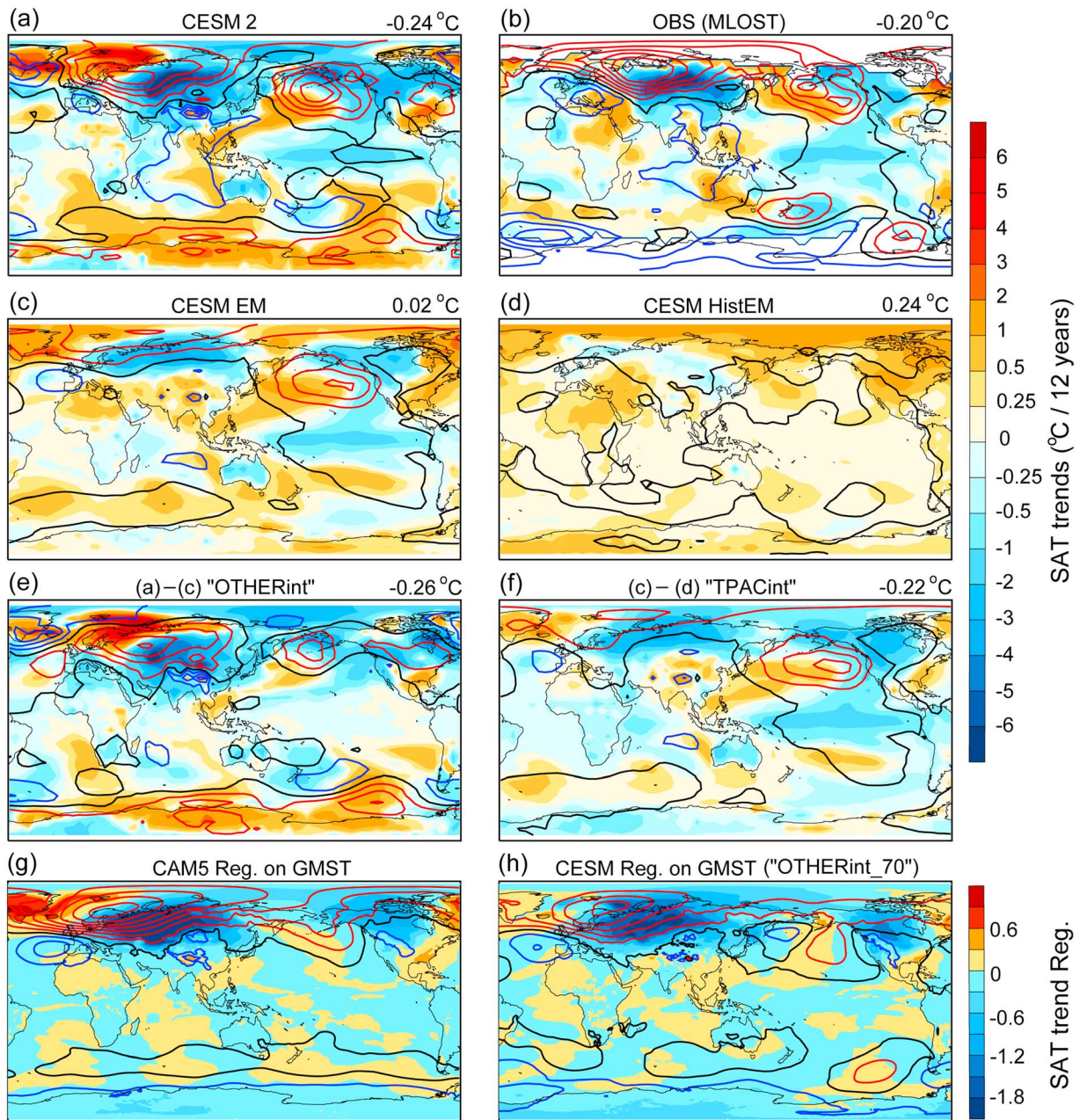


Figure 4. (a and b) DJF SAT and SLP trends (2002–2013; $^{\circ}\text{C}/12 \text{ years}$ and $\text{hPa}/12 \text{ years}$) from CSM1 Pacemaker ensemble member #2 (CESM 2) and observations, respectively. The SLP contour interval is 2 $\text{hPa}/12 \text{ years}$, with positive (negative) values in red (blue) and the zero contour in black. (c and d) Same as in Figure 4a but for the ensemble mean of the 10 CSM1 Pacemaker simulations (CESM EM) and the 40 CSM1 historical simulations (CESM HistEM), respectively. (e) Figure 4a minus Figure 4c, termed "OTHERint" in the text. (f) Figure 4c minus Figure 4d, termed "TPACint" in the text. (g) The 12 year trend regressions of SAT ($^{\circ}\text{C}$ per unit standard deviation of GMST; color shading) and SLP (contour interval = 0.5 hPa per unit standard deviation of GMST) on standardized GMST trends from the 2600 year CAM5 control simulation. (h) Same as in Figure 4g but from the CSM1 Pacemaker ensemble over the period of 1920–2013 after removing the ensemble mean trend for each 12 year segment (termed "OTHERint_70" in the text).

Notably, none of the CM2.1 ensemble members simulate Eurasian cooling trends in excess of -0.5°C , which is less than 25% of the observed value of -2.2°C (Figure S4).

Given the close correspondence between CSM1 member 2 (hereafter CSM1_#2) and observations in terms of all metrics examined (GMST and Eurasian SAT trends, pattern correlation, and RMSE), we investigate the various factors contributing to the global pattern of SAT trends in this particular simulation. We begin by

examining the association between atmospheric circulation and SAT trends. Both CESM1_#2 and observations (ERA-I) show positive SLP trends over western Eurasia and the North Pacific of similar magnitude, consistent with the notion that atmospheric circulation trends cause the cooling trends over Eurasia and North America through anomalous cold air advection (Figures 4a and 4b, respectively). To what extent are the SLP and SAT trends in CESM1_#2 forced by tropical Pacific SSTA versus radiative changes? The CESM1_EM, which includes both effects, also shows positive SLP anomalies in these locations but with reduced amplitude, in accordance with the weaker cooling over the continents, compared to CESM1_#2 (Figure 4c). The SLP and SAT responses in CESM1_EM, in turn, are primarily a result of internal variability driven by tropical Pacific SST changes (Figure 4f) rather than radiative forcing (Figure 4d), the latter obtained from the ensemble mean of the 40 CESM1 historical/RCP simulations (CESM1_HistEM) and the former obtained by subtracting CESM1_HistEM from CESM1_EM (hereafter referred to as "TPACint"). However, radiative forcing makes a slight contribution to the cooling over central Eurasia and Scandinavia; this cooling is also circulation-induced via a weak positive SLP trend to the north (evident by comparing the number of SLP contours in Figures 4c and 4f; see also Figure S5). Analogous maps to Figures 4c, 4d, and 4f based on CM2.1 are provided in Figure S6 and discussed in the supporting information.

How much do observed tropical Pacific SST changes versus other sources of (model-generated) internal variability contribute to the trends in CESM1_#2? To answer this question, we compare CESM1_#2 (Figure 4a) with TPACint (Figure 4f) and with the residual of CESM1_#2 from CESM1_EM (hereafter termed "OTHERint"; Figure 4e). TPACint is responsible for most of the positive SLP trends over the northeastern Pacific and the Arctic, with associated cooling over North America and northern Eurasia. However, OTHERint accounts for the positive SLP trends over Eurasia and Canada, which in turn cause most of the cooling in central Eurasia (and warming in the Barents and Kara Seas) and contribute to cooling in Canada. In terms of the GMST trend in CESM1_#2 (-0.24°C), TPACint and OTHERint contribute -0.22°C and -0.26°C , respectively, and together more than offset the radiatively induced warming trend of $+0.24^{\circ}\text{C}$ (Table S1 in the supporting information).

Are the OTHERint SLP and SAT trends in CESM1_#2 a general feature of CESM1's internal variability or specific to this particular ensemble member? To address this question, we form 12 year trends from nonoverlapping segments of each CESM1 Pacemaker simulation using the full period of record (1920–2013), for a total of seven trend values for each of the 10 ensemble members. We then compute the ensemble-mean trend value for each segment, and then subtract this value from the trend of the corresponding segment in each simulation. In this way, we isolate the component of each of the 70 trend values that arises from internal variability beyond that generated by the tropical Pacific. Finally, we concatenate all 70 trend values to form a grand ensemble, hereafter referred to as "OTHERint_70." This procedure is performed at each grid box separately.

What SLP and SAT trend patterns are most commonly associated with a 12 year trend in GMST in OTHERint_70? Figure 4h shows the results of regressing the 12 year SLP and SAT trends at each grid box on the normalized 12 year GMST trends in OTHERint_70, where the signs have been reversed to facilitate visual comparison with the other plots in Figure 4 (the analogous regression map for CM2.1 is shown in Figure S6d and discussed in the supporting information). On average, a negative 1 standard deviation departure of a 12 year trend in GMST is associated with cooling over Eurasia and most of North America, and slight warming over Greenland, the southeastern U.S., and Mexico, in addition to high-latitude positive SLP trends, with largest amplitudes centered over northwestern Eurasia (Figure 4h). A positive 1 standard deviation departure of the GMST trend is associated with opposite-signed changes. The lack of appreciable regression amplitudes over ocean indicates that this pattern of internal variability is unlikely to originate from the ocean or the coupled ocean-atmosphere system.

To test this notion, we make use of the 2600 year control integration of the atmosphere-land model (hereafter referred to as CAM5). Recall from section 2 that this control integration has no variability in SSTs or sea ice, and thus, any variability derives mainly from intrinsic atmospheric dynamics. Following an analogous procedure to that used for OTHERint_70, we compute 12 year trends from nonoverlapping segments of the CAM5 control run, for a total of 216 segments. The resulting SLP and SAT trend regression maps, formed by regressing the 216 trend values at each grid box on the 216 GMST trend values, are shown in Figure 4g. That the SLP and SAT trend regression patterns in the CAM5 control simulation are very similar to those in OTHERint_70 based on the fully coupled CESM1 (compare Figures 4g and 4h) strongly suggests that the

latter is derived largely from intrinsic atmospheric dynamics. Furthermore, the overall resemblance between the patterns in OTHERint_70 (Figure 4e) and CAM5 (Figure 4g), apart from some small differences in exact location, suggests that intrinsic atmospheric dynamics are responsible for the substantial trends in SAT and SLP that remain in CESM1_#2 after the effects of radiative forcing and observed internally generated tropical Pacific SST changes are removed.

4. Summary and Discussion

We have examined the relative contributions of radiative forcing, observed tropical Pacific SST variability, and other internal variability to the recent hiatus in global-mean surface warming during boreal winter using two global coupled climate models subject to the same experimental protocols. The model simulations include 10-member initial-condition ensembles in which observed tropical Pacific SSTA and radiative forcings are specified (the so-called “Pacemaker” simulations). We focus on the fidelity with which the Pacemaker simulations replicate the observed spatial distribution of SAT trends during the hiatus, in addition to the global mean trend. We find considerable diversity in pattern and amplitude of SAT trends across the 10 individual ensemble members in both models, attesting to the importance of internal variability beyond the tropical Pacific that is superimposed upon the response to TPAC SSTA and radiative forcing. In CESM1, the ensemble members with the most realistic patterns also show the highest fidelity in their SAT amplitudes and GMST. In CM2.1, however, the members with the most realistic GMST trends show relatively high RMSE and low pattern correlation with respect to observations. No single member of the CM2.1 ensemble replicates the observed spatial pattern and amplitude of SAT trends as well as CESM1. Relatedly, Eurasian SAT trends play a negligible role in determining the amplitude of the GMST trend in the CM2.1 ensemble, opposite to that found in nature and the CESM1 ensemble. These results highlight that conclusions about a model’s ability to simulate the hiatus in terms of GMST may not extend to its ability to simulate the associated geographical pattern of SAT trends.

Like observations, the most realistic Pacemaker simulation (CESM1_#2) shows positive SLP trends centered over western Eurasia and the North Pacific; this anomalous atmospheric circulation is indicative of cold air advection, consistent with the cooling trends over Eurasia and North America. In the model, we can identify the contributions of radiative forcing, observed tropical Pacific SSTA, and internal variability arising from other sources to these NH SAT and SLP trends. We find that circulation-driven cooling over northern Eurasia and North America results from atmospheric teleconnections forced by the tropical Pacific, with the most of the remaining cooling over central Eurasia and North America due to other sources, likely intrinsic atmospheric dynamics. Radiatively forced warming partially counteracts the dynamically induced cooling via thermodynamic processes; however, it augments the cooling over central Eurasia via circulation changes. In terms of GMST trend, the two sources of internal variability contribute approximately equally. A similar result is found for the observed GMST trend using the CESM1 GMST responses to radiative forcing and observed tropical Pacific SSTA (Table S1). While the model-based results do not prove a chain of causality in the real world, they are highly suggestive given the realism of CESM1_#2 in many key aspects of the hiatus.

Larger ensembles of Pacemaker simulations with these and other models, and analyses that pay particular attention to the fidelity of the spatial pattern of SAT trends that produce the GMST trend, are needed to further our understanding of the observed hiatus. Verification of the models’ responses to radiative forcing and tropical Pacific SST trends against the short observational record remains an outstanding challenge.

Acknowledgments

We thank Tingting Fan for carrying out the CESM1 Pacemaker experiments and Yu Kosaka for sharing the GFDL CM2.1 model output. R.G. was supported by China Scholarship Council and F.L. by a Postdoc Applying Climate Expertise fellowship cosponsored by NOAA and the Bureau of Reclamation. NCAR is sponsored by the National Science Foundation. The CESM simulations are available on the Earth System Grid (www.earthsystemgrid.org/); contact Y. Kosaka (ykosaka@atmos.rcast.u-tokyo.ac.jp) for the CM2.1 simulations. We thank the reviewers and the Editor for their constructive comments and suggestions.

References

- Chen, X. Y., and K. K. Tung (2014), Varying planetary heat sink led to global-warming slowdown and acceleration, *Science*, *345*, 897–903, doi:10.1126/science.1254937.
- Cohen, J. L., J. C. Furtado, M. A. Barlow, V. A. Alexeev, and J. E. Cherry (2012), Arctic warming, increasing fall snow cover and widespread boreal winter cooling, *Environ. Res. Lett.*, *7*, 014007, doi:10.1088/1748-9326/7/1/014007.
- Dai, A. G., J. C. Fyfe, S. P. Xie, and X. G. Dai (2015), Decadal modulation of global surface temperature by internal climate variability, *Nat. Clim. Change*, *5*, 555–559, doi:10.1038/nclimate2605.
- Dee, D. P., et al. (2011), The ERA-interim reanalysis: Configuration and performance of the data assimilation system, *Q. J. R. Meteorol. Soc.*, *137*, 553–597, doi:10.1002/qj.828.
- Deser, C., I. R. Simpson, K. A. McKinnon, and A. S. Phillips (2017), The Northern Hemisphere Extra-Tropical Atmospheric Circulation Response to ENSO: How Well Do We Know It and How Do We Evaluate Models Accordingly?, *J. Clim.*, *30*, 5059–5082, doi:10.1175/JCLI-D-16-0844.1.
- Douville, H., A. Voldoire, and O. Geoffroy (2015), The recent global warming hiatus: What is the role of Pacific variability?, *Geophys. Res. Lett.*, *42*, 880–888, doi:10.1002/2014GL062775.

- England, M. H., S. McGregor, P. Spence, G. A. Meehl, A. Timmermann, W. J. Cai, A. S. Gupta, M. J. McPhaden, A. Purich, and A. Santoso (2014), Recent intensification of wind-driven circulation in the Pacific and the ongoing warming hiatus, *Nat. Clim. Change*, *4*, 222–227, doi:10.1038/nclimate2106.
- Fyfe, J. C., et al. (2016), Making sense of the early-2000s warming slowdown, *Nat. Clim. Change*, *6*, 224–228, doi:10.1038/nclimate2938.
- Hu, S., and A. V. Fedorov (2017), The extreme El Niño of 2015–2016 and the end of global warming hiatus, *Geophys. Res. Lett.*, *44*, 3816–3824, doi:10.1002/2017GL072908.
- Huang, J. P., Y. K. Xie, X. D. Guan, D. D. Li, and F. Ji (2017), The dynamics of the warming hiatus over the northern hemisphere, *Clim. Dyn.*, *48*, 429–446, doi:10.1007/s00382-016-3085-8.
- Huber, M., and R. Knutti (2014), Natural variability, radiative forcing and climate response in the recent hiatus reconciled, *Nat. Geosci.*, *7*, 651–656, doi:10.1038/ngeo2228.
- Kay, J. E., et al. (2015), The Community Earth System Model (CESM) large ensemble project a community resource for studying climate change in the presence of internal climate variability, *Bull. Am. Meteorol. Soc.*, *96*, 1333–1349, doi:10.1175/bams-d-13-00255.1.
- Kosaka, Y., and S. P. Xie (2013), Recent global-warming hiatus tied to equatorial Pacific surface cooling, *Nature*, *501*, 403–407, doi:10.1038/nature12534.
- Kosaka, Y., and S. P. Xie (2016), The tropical Pacific as a key pacemaker of the variable rates of global warming, *Nat. Geosci.*, *9*, 669–673, doi:10.1038/ngeo2770.
- Li, C., B. Stevens, and J. Marotzke (2015), Eurasian winter cooling in the warming hiatus of 1998–2012, *Geophys. Res. Lett.*, *42*, 8131–8139, doi:10.1002/2015GL065327.
- Luo, D. H., Y. Q. Xiao, Y. Yao, A. G. Dai, I. Simmonds, and C. L. E. Franzke (2016), Impact of Ural blocking on winter warm Arctic–cold Eurasian anomalies. Part I: Blocking-induced amplification, *J. Clim.*, *29*, 3925–3947, doi:10.1175/JCLI-D-15-0611.1.
- Mantua, N. J., S. R. Hare, Y. Zhang, J. M. Wallace, and R. C. Francis (1997), A Pacific interdecadal climate oscillation with impacts on salmon production, *Bull. Am. Meteorol. Soc.*, *78*, 1069–1079, doi:10.1175/1520-0477(1997)078<1069:APICOW>2.0.CO;2.
- Marotzke, J., and P. M. Forster (2015), Forcing, feedback and internal variability in global temperature trends, *Nature*, *517*, 565–570, doi:10.1038/nature14117.
- Power, S., T. Casey, C. K. Folland, and V. M. Mehta (1999), Inter-decadal modulation of the impact of ENSO on Australia, *Clim. Dyn.*, *15*, 319–324, doi:10.1007/s003820050284.
- Saffioti, C., E. M. Fischer, and R. Knutti (2015), Contributions of atmospheric circulation variability and data coverage bias to the warming hiatus, *Geophys. Res. Lett.*, *42*, 2385–2391, doi:10.1002/2015GL063091.
- Smith, T. M., R. W. Reynolds, T. C. Peterson, and J. Lawrimore (2008), Improvements to NOAA's historical merged land-ocean surface temperature analysis (1880–2006), *J. Clim.*, *21*, 2283–2296, doi:10.1175/2007JCLI2100.1.
- Taylor, K. E., R. J. Stouffer, and G. A. Meehl (2012), An overview of CMIP5 and the experiment design, *Bull. Am. Meteorol. Soc.*, *93*, 485–498, doi:10.1175/BAMS-D-11-00094.1.
- Trenberth, K. E., J. T. Fasullo, G. Branstator, and A. S. Phillips (2014), Seasonal aspects of the recent pause in surface warming, *Nat. Clim. Change*, *4*, 911–916, doi:10.1038/nclimate2341.
- Vose, R. S., et al. (2012), NOAA's merged land-ocean surface temperature analysis, *Bull. Am. Meteorol. Soc.*, *93*, 1677–1685, doi:10.1175/BAMS-D-11-00241.1.
- Watanabe, M., H. Shiogama, H. Tatebe, M. Hayashi, M. Ishii, and M. Kimoto (2014), Contribution of natural decadal variability to global warming acceleration and hiatus, *Nat. Clim. Change*, *4*, 893–897, doi:10.1038/nclimate2355.